

# Electric-field induced half-metal in monolayer CrSBr

Hao-Tian Guo<sup>1</sup>, San-Dong Guo<sup>1\*</sup> and Yee Sin Ang<sup>2</sup>

<sup>1</sup>*School of Electronic Engineering, Xi'an University of Posts and Telecommunications, Xi'an 710121, China and*

<sup>2</sup>*Science, Mathematics and Technology (SMT), Singapore University of Technology and Design (SUTD), 8 Somapah Road, Singapore 487372, Singapore*

Two-dimensional (2D) half-metallic materials are highly desirable for nanoscale spintronic applications. Here, we propose a new mechanism that can achieve half-metallicity in 2D ferromagnetic (FM) material with two-layer magnetic atoms by electric field tuning. We use a concrete example of experimentally synthesized CrSBr monolayer to illustrate our proposal through the first-principle calculations. It is found that the half-metal can be achieved in CrSBr within appropriate electric field range, and the corresponding amplitude of electric field intensity is available in experiment. Janus monolayer Cr<sub>2</sub>S<sub>2</sub>BrI is constructed, which possesses built-in electric field due to broken horizontal mirror symmetry. However, Cr<sub>2</sub>S<sub>2</sub>BrI without and with applied external electric field is always a FM semiconductor. A possible memory device is also proposed based on CrSBr monolayer. Our works will stimulate the application of 2D FM CrSBr in future spintronic nanodevices.

Keywords: Half-metal, Monolayer, Electric field

Email:sandongyuwang@163.com

## INTRODUCTION

Spintronics provides a promising solution for developing information technology with high speed and low energy consumption by using the spin degrees of freedom of electrons[1]. The half-metallic ferromagnets, where one spin channel is conducting while the other spin channel is insulating or semiconducting, possess 100% spin polarized carriers around the Fermi level, which are highly desired for high-performance spintronic devices by filtering the current into a single spin channel for realizing pure spin generation, injection, and transport[2]. The three-dimensional (3D) half-metals have been widely investigated both in theory and in experiment[3]. In order to realize higher integration density, two-dimensional (2D) half-metallic ferromagnets may be preferred. Although a number of 2D magnets have been obtained experimentally[4–6], a 2D ferromagnetic (FM) half-metal is still missing.

Although there are various theoretical proposals of 2D half-metals[7–9], no experimental evidence to prove the existence of intrinsic 2D half-metallicity has been reported. Fortunately, bilayer A-type antiferromagnetic (AFM) materials (intralayer FM ordering and interlayer AFM ordering) can be used to produce half-metallic properties by applying the out-of-plane electric field[10, 11]. The underlying mechanism is that the applied electric field makes the electrostatic potential of one constituent layer rise and that of the other layer decrease, giving rise to a semiconductor-metal phase transition. This strategy can also be used to realize the control of spin polarization in 2D A-type AFM semiconductors[12]. Besides, the ferrovalley metal (FVM) and valley gapless semiconductor (VGS) can also be achieved in valleytronic bilayer AFM systems by electric field tuning[13].

A natural question is whether this strategy or mechanism can be applied to 2D FM systems. Here, we propose

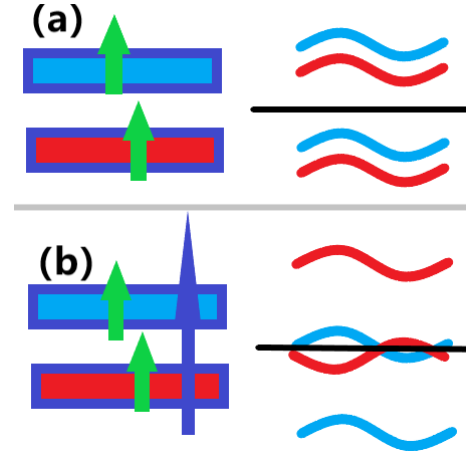


FIG. 1. (Color online) (a): for a 2D material, the magnetic atoms have the same layer spin polarization, and the energy bands near the Fermi level are from the same spin channel, which have different layer character for both valence and conduction bands. (b): when an out-of-plane electric field is applied, the electronic bands in different layers will stagger, which can induce half-metal. The green arrows mean spin, while the blue arrow shows an out-of-plane electric field. The black horizontal lines mean Fermi level.

a new mechanism that can achieve half-metallicity in 2D FM material with two-layer magnetic atoms by electric field tuning (see Figure 1). For a 2D material, the two-layer magnetic atoms have the FM coupling, and the energy bands near the Fermi level are from the same spin channel with different layer character for both valence and conduction bands. When an out-of-plane electric field is applied, the electronic bands in different layers will stagger, resulting in a half-metal. To illustrate our proposal, a concrete example is experimentally synthesized CrSBr monolayer[14], and both crystal structures and energy band structures meet the above requirements[15–17]. Calculated results show that the half-metal can in-

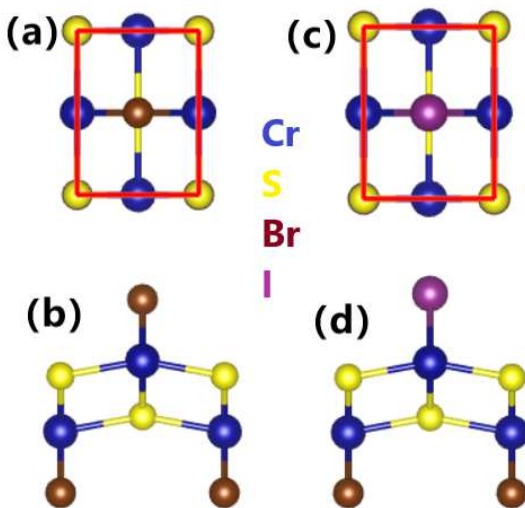


FIG. 2. (Color online) For monolayer CrSBr (a,b) and Janus monolayer Cr<sub>2</sub>S<sub>2</sub>BrI (c,d): top (a,c) and side (b,d) views of the crystal structures.

deed be achieved in CrSBr within appropriate electric field range, and the corresponding amplitude of electric field intensity is available in experiment ( $\sim 0.4 \text{ V/\AA}$ [18]). Our results pave the way for the realization and application of 2D half-metal in future spintronic nanodevices.

### COMPUTATIONAL DETAIL

Spin-polarized first-principles calculations are carried out within density functional theory (DFT)[19] by the projector augmented-wave (PAW) method, as implemented in the Vienna ab initio simulation package (VASP)[20–22]. We use the generalized gradient approximation of Perdew-Burke-Ernzerhof (PBE-GGA)[23] as the exchange-correlation functional. The kinetic energy cutoff of 500 eV, total energy convergence criterion of  $10^{-8}$  eV, and force convergence criterion of  $0.001 \text{ eV.\AA}^{-1}$  are set to obtain accurate results. To account for electron correlation of Cr-3d orbitals, a Hubbard correction  $U_{eff}=3.00 \text{ eV}$ [15–17] is employed within the rotationally invariant approach proposed by Dudarev et al. To avoid out-of-plane interaction, a vacuum of more than  $16 \text{ \AA}$  is adopted. We use a  $18 \times 14 \times 1$  Monkhorst-Pack k-point meshes to sample the Brillouin zone (BZ) for calculating electronic structures, elastic and piezoelectric properties. The elastic stiffness tensor  $C_{ij}$  and piezoelectric stress tensor  $e_{ij}$  are calculated by using strain-stress relationship (SSR) method and density functional perturbation theory (DFPT)[24], respectively. The  $C_{ij}^{2D}/e_{ij}^{2D}$  have been renormalized by  $C_{ij}^{2D}=L_z C_{ij}^{3D}/e_{ij}^{2D}=L_z e_{ij}^{3D}$ , where the  $L_z$  is the length of unit cell along  $z$  direction. The interatomic force constants (IFCs) are obtained by using  $4 \times 4 \times 1$  supercell within finite displacement method,

and then calculate phonon dispersion spectrum by the Phonopy code[25].

### MAIN RESULTS

Monolayer CrSBr possesses an orthorhombic crystal structure with a space group of  $Pmmn$  (No.59)[14], which has two distinct in-plane crystallographic directions (see Figure 2 (a) and (b)). The CrSBr includes six atomic layers in the sequence of Br-Cr-S-S-Cr-Br. The magnetic Cr atoms distribute in two layers, which reside in distorted octahedral coordination formed by S and Br atoms. The lattice constants of CrSBr with FM ordering are obtained by GGA+ $U$ , and the corresponding values  $a=3.584 \text{ \AA}$  and  $b=4.825 \text{ \AA}$ .

Electric field is a very effective way to tune electronic structures, topological properties and magnetic anisotropy energy of 2D materials[10–13, 26–28]. Here, the electric field effects on magnetic properties and electric structures in CrSBr are investigated. Firstly, we determine the magnetic ground state under the electric field, and four magnetic configurations (FIG.1 of electronic supplementary information (ESI)) are considered, including FM case and three AFM cases (AFM, AFM-x and AFM-y). The energy differences per formula unit between AFM/AFM-x/AFM-y and FM as a function of electric field  $E$  are shown in FIG.2 of ESI. For AFM-x case, the result converges to a non-magnetic state, which leads to very high energy. Calculated results show that the FM state is always ground state within considered  $E$  range.

The energy band structures of CrSBr under representative  $E$  are shown in Figure 3, and the global gap ( $G_T$ ) and the energy difference ( $G_\Gamma$ ) at  $\Gamma$  point for the first two conduction bands as a function of  $E$  are plotted in Figure 4. Without electric field, CrSBr is a FM semiconductor with gap value of  $0.865 \text{ eV}$ , and the valence band maximum (VBM) and conduction band bottom (CBM) are at  $\Gamma$  and one point close to X, which are from the same spin-up channel. This provides possibility to achieve half-metal in CrSBr by electric field tuning. With increasing  $E$ , the global gap decreases, and a semiconductor-metal phase transition can be observed at about  $E=0.38 \text{ V/\AA}$ . At about  $E=0.55 \text{ V/\AA}$ , a gap of  $24 \text{ meV}$  is produced, meaning a metal-semiconductor phase transition. Calculated results show that  $G_\Gamma$  firstly increases, and then decreases. For  $0.38 \text{ V/\AA} < E < 0.55 \text{ V/\AA}$ , 2D half-metal can be realized in CrSBr. Here, we define half-metallic gap  $G_{HM}$  as the smaller of  $E_{cb}$  and  $E_{vt}$ , where  $E_{cb}/E_{vt}$  is the bottom/top energy of the spin-down conduction/valence bands with respect to the Fermi (absolute value), which is rough estimates for the minimal energy for spin flip excitation. The  $G_{HM}$  vs  $E$  is plotted in FIG.3 of ESI, which are all larger than  $0.33 \text{ eV}$ .

This out-of-plane electric field creates a layer-

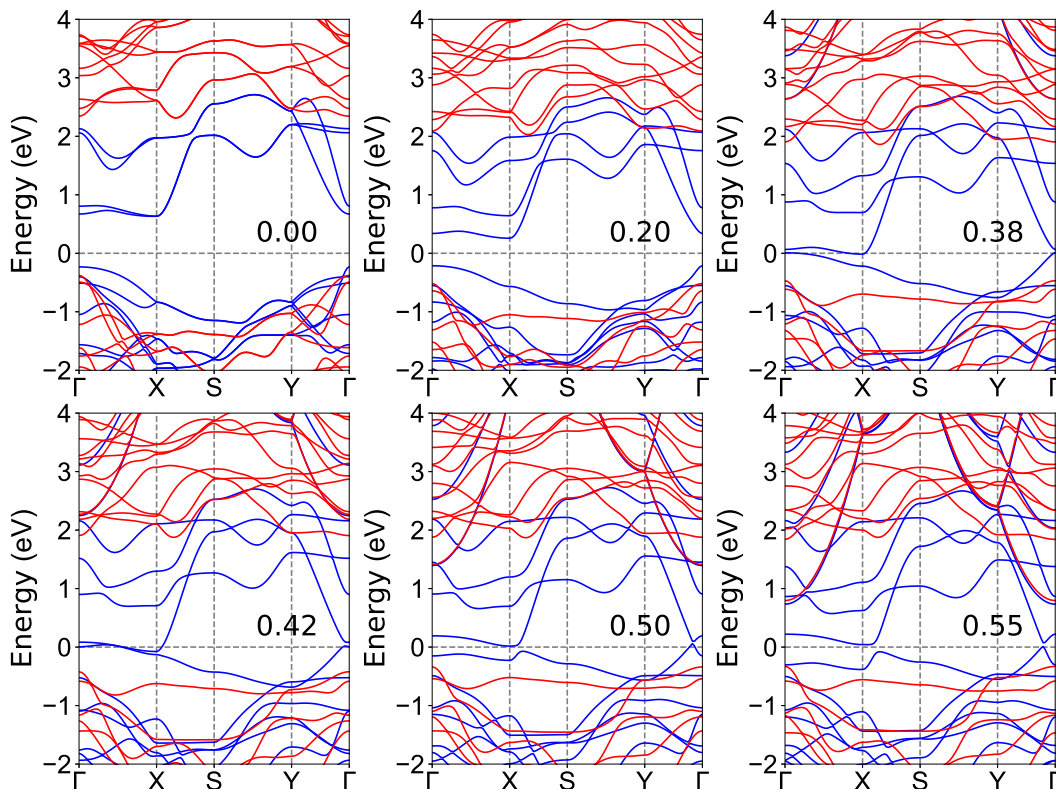


FIG. 3. (Color online) The energy band structures of CrSBr at representative electric field  $E$ . The spin-up and spin-down channels are depicted in blue and red. An appropriate electric field intensity can induce half-metal, for example  $E=0.42$  V/Å.

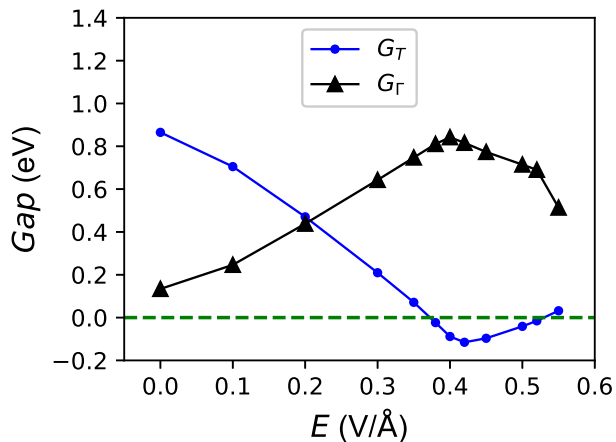


FIG. 4. (Color online) For CrSBr, the global gap ( $G_T$ ) and the energy difference ( $G_\Gamma$ ) at  $\Gamma$  point for the first two conduction bands as a function of  $E$ .

dependent electrostatic potential[10–13], and the electronic bands in different Cr layers will stagger, which gives rise to half-metallic property in CrSBr. To clearly see this, two Cr layer-characters energy band structures are plotted in FIG.4 of ESI at  $E=0.35$  V/Å and  $0.42$  V/Å, which shows that the energy band from down-layer Cr is shifted toward higher energy with respect to one of

up-layer. Experimentally, the CrSBr monolayer has been achieved[14]. Recently, an intense electric field larger than  $0.4$  V/Å has been realized in 2D materials by dual ionic gating[18]. These provide very good foundation to experimentally produce half-metallic property in CrSBr.

The out-of-plane built-in electric field is equivalent to an external electric field[29]. The CrSBr possesses spatial centrosymmetry, producing no built-in electric field. Here, Janus monolayer  $\text{Cr}_2\text{S}_2\text{BrI}$  is constructed by replacing one of two Br layers with I atoms in monolayer CrSBr. The schematic crystal structures of  $\text{Cr}_2\text{S}_2\text{BrI}$  are shown in Figure 2 (c) and (d), which has  $Pmm2$  space group (No.25). Due to broken horizontal mirror symmetry, an out-of-plane built-in electric field can be produced in  $\text{Cr}_2\text{S}_2\text{BrI}$ . The energy differences between AFM/AFM-x/AFM-y and FM configurations is  $0.097/0.095/0.070$  eV, and the positive values confirm that  $\text{Cr}_2\text{S}_2\text{BrI}$  is FM ground state. The optimized lattice constant  $a$  and  $b$  are  $3.662$  Å and  $4.816$  Å with FM ordering by GGA+ $U$ .

To verify its dynamical stability, the phonon dispersions of  $\text{Cr}_2\text{S}_2\text{BrI}$  is calculated, as shown in FIG.5 of ESI. No obvious imaginary frequencies are observed in the whole BZ, implying that  $\text{Cr}_2\text{S}_2\text{BrI}$  is dynamically stable. To further confirm its thermal stability, the ab-initio molecular dynamics (AIMD) simulations are carried out

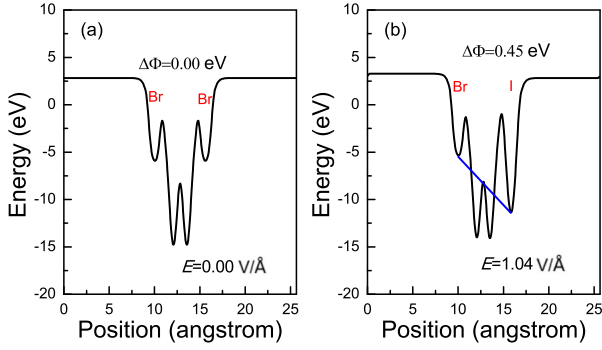


FIG. 5. (Color online) For monolayer CrSBr (a) and  $\text{Cr}_2\text{S}_2\text{BrI}$  (b), the planar averaged electrostatic potential energy variation along  $z$  direction.  $\Delta\Phi$  is the potential energy difference across the layer.  $E$  means built-in electric field.

with a  $4 \times 3 \times 1$  supercell and a time step of 1 fs at 300 K for 8 ps. According to FIG.6 of ESI, the energy fluctuates within a small range during the whole simulation time, and the snapshot shows no structural transitions at the end of the AIMD simulations, which manifest its thermal stability. The linear elastic constants can be used to determine the mechanical stability of  $\text{Cr}_2\text{S}_2\text{BrI}$ . Due to  $Pmm2$  space group, there are four independent elastic constants:  $C_{11} = 81.37 \text{ Nm}^{-1}$ ,  $C_{12} = 9.48 \text{ Nm}^{-1}$ ,  $C_{22} = 98.57 \text{ Nm}^{-1}$  and  $C_{66} = 21.36 \text{ Nm}^{-1}$ , which meet Born-Huang criteria of mechanical stability ( $C_{11} > 0$ ,  $C_{22} > 0$ ,  $C_{66} > 0$  and  $C_{11} - C_{12} > 0$ ), thereby verifying its mechanical stability.

The planar average of the electrostatic potential energy of CrSBr and  $\text{Cr}_2\text{S}_2\text{BrI}$  along  $z$  direction are shown in Figure 5. An electrostatic potential gradient ( $\Delta\Phi$ ) is related to the work function change of the structure. Due to horizontal mirror symmetry,  $\Delta\Phi$  and inherent electric field of CrSBr are zero. Due to mirror asymmetry of  $\text{Cr}_2\text{S}_2\text{BrI}$ , there is an inherent electric field with the magnitude of about  $1.04 \text{ V/\AA}$ , and  $\Delta\Phi$  of about 0.45 eV, which are due to the electron redistribution caused by different electronegativity of Br and I atoms. The magnitude of inherent electric field for  $\text{Cr}_2\text{S}_2\text{BrI}$  is larger than an external electric field, which can make CrSBr become a half-metal.

Next, the electronic structures of  $\text{Cr}_2\text{S}_2\text{BrI}$  along with electric field effects are investigated. Due to mirror asymmetry of  $\text{Cr}_2\text{S}_2\text{BrI}$ , the electric fields along the  $+z$  and  $-z$  directions are not equivalent. The energy differences per formula unit between AFM/AFM-x/AFM-y and FM orderings as a function of electric field  $E$  are shown in FIG.7 of ESI, which shows that the FM state is always ground state of  $\text{Cr}_2\text{S}_2\text{BrI}$  within considered  $E$  range. The energy band structures of  $\text{Cr}_2\text{S}_2\text{BrI}$  under representative  $E$  are shown in FIG.8 and FIG.9 of ESI, and the global gap ( $G_T$ ) and the energy difference ( $G_\Gamma$ ) at  $\Gamma$  point for the first two conduction bands as a function of  $E$  are

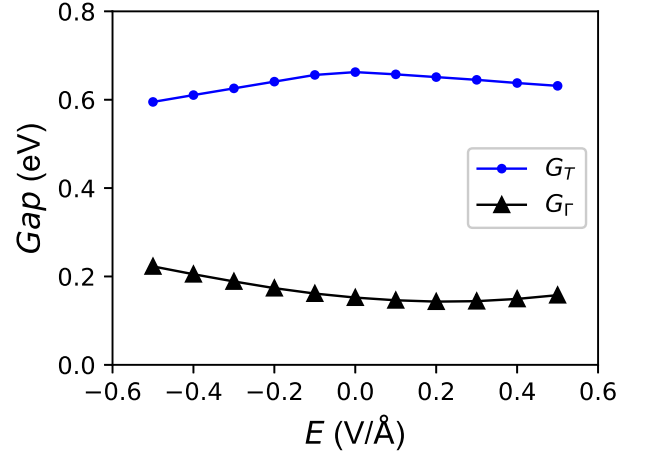


FIG. 6. (Color online) For  $\text{Cr}_2\text{S}_2\text{BrI}$ , the global gap ( $G_T$ ) and the energy difference ( $G_\Gamma$ ) at  $\Gamma$  point for the first two conduction bands as a function of  $E$ .

plotted in Figure 6. Without electric field,  $\text{Cr}_2\text{S}_2\text{BrI}$  is still a FM semiconductor with gap value of 0.663 eV, and the VBM and CBM are at  $\Gamma$  and one point close to X, which are from the same spin-up channel. These are very similar to those of CrSBr. Calculated results show that no semiconductor-metal phase transition is produced within considered  $E$  range ( $-0.5 \text{ V/\AA}$  to  $0.5 \text{ V/\AA}$ ). It is found that electric field has small effects on  $G_T$  and  $G_\Gamma$  of  $\text{Cr}_2\text{S}_2\text{BrI}$ . Therefore, it is not possible to achieve half-metal by building Janus structures with built-in electric field.

However, compared with CrSBr,  $\text{Cr}_2\text{S}_2\text{BrI}$  possesses piezoelectricity due to broken spatial inversion symmetry. By using Voigt notation, only considering the in-plane strain and stress[30], the piezoelectric stress and strain tensors of  $\text{Cr}_2\text{S}_2\text{BrI}$  can be written as:

$$e = \begin{pmatrix} 0 & 0 & 0 \\ 0 & 0 & 0 \\ e_{31} & e_{32} & 0 \end{pmatrix} \quad (1)$$

$$d = \begin{pmatrix} 0 & 0 & 0 \\ 0 & 0 & 0 \\ d_{31} & d_{32} & 0 \end{pmatrix} \quad (2)$$

The  $e_{31}$  and  $e_{32}$  can be attained by DFPT, and the  $d_{31}$  and  $d_{32}$  can be derived by  $e_{ik} = d_{ij} C_{jk}$ :

$$d_{31} = \frac{e_{31}C_{22} - e_{32}C_{12}}{C_{11}C_{22} - C_{12}^2} \text{ and } d_{32} = \frac{e_{32}C_{11} - e_{31}C_{12}}{C_{11}C_{22} - C_{12}^2} \quad (3)$$

The calculated  $e_{31}/e_{32}$  is  $0.708 \times 10^{-10} / 0.016 \times 10^{-10} \text{ C/m}$ . And then, the  $d_{31}/d_{32}$  of  $\text{Cr}_2\text{S}_2\text{BrI}$  can be attained from Equation 3, and the corresponding value is 0.878/-0.068 pm/V, showing very strong in-plane anisotropy. The  $d_{31}$  of  $\text{Cr}_2\text{S}_2\text{BrI}$  is compared with or higher than ones of many known 2D materials[30–34].



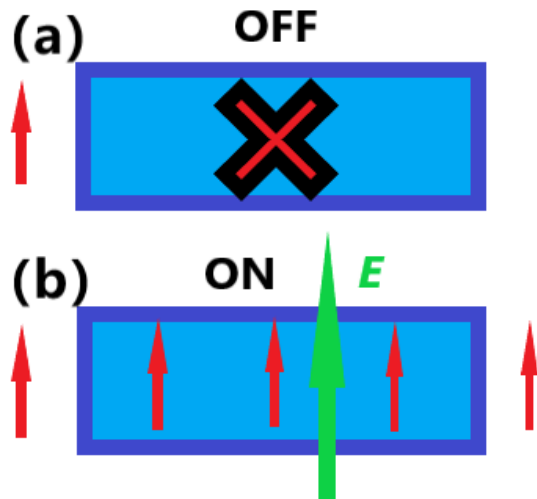


FIG. 7. (Color online) Schematic of a possible spintronic device. The red arrows represent spin, while the green arrow represents an out-of-plane electric field.

## DISCUSSION AND CONCLUSION

The half-metallic property can be induced by applied out-of-plane electric field in CrSBr, which provides a possibility to realize memory device (see Figure 7). For example, two FM electrodes are set in the same direction for source and drain electrodes. Without the out-of-plane electric field, no electrons can propagate through the CrSBr due to semiconducting property (“off” state) (Figure 7 (a)). When an appropriate out-of-plane external electric field is applied, spin-up electrons can propagate through the CrSBr because of half-metallic property (“on” state) (Figure 7 (b)). Here, data writing in the memory is realized by turning on and off out-of-plane external electric field, and data reading is realized by detecting the electrical signals.

In summary, a new mechanism is proposed to achieve half-metallicity in 2D FM systems with two-layer magnetic atoms by electric field tuning. A concrete example of experimentally synthesized CrSBr monolayer is used to illustrate our proposal through the first-principle calculations. The half-metal can indeed be achieved in CrSBr within experimentally available electric field range. Janus monolayer Cr<sub>2</sub>S<sub>2</sub>BrI is constructed with built-in electric field, but it can not be used to induce half-metallic property. In fact, our work provides a feasible and general approach to achieve half-metal. The method, analysis and results can be readily extended to VSF, VSeF, VSeBr, CrSCl, CrSI, CrSeBr and CrSeI[35], which have the same structure and FM configuration with CrSBr. Based on these monolayers, an applied vertical electric field can realize half-metal.

## SUPPLEMENTARY MATERIAL

See the supplementary material for magnetic configura-

tions; the energy difference between AFM and FM ordering; half-metallic gap; the related energy band structures; the phonon dispersions and AIMD results.

## Conflicts of interest

There are no conflicts to declare.

This work is supported by Natural Science Basis Research Plan in Shaanxi Province of China (2021JM-456). We are grateful to Shanxi Supercomputing Center of China, and the calculations were performed on TianHe-2.

- 
- [1] S. A. Wolf, D. D. Awschalom, R. A. Buhrman, M. Daughton, S. von Molnar, M. L. Roukes, A. Y. Chtchelkanova and D. M. Treger, *Science* **294**, 1488 (2001).
  - [2] R. A. de Groot, F. M. Mueller, P. G. van Engen and K. H. J. Buschow, *Phys. Rev. Lett.* **50**, 2024 (1983).
  - [3] M. I. Katsnelson, V. Yu. Irkhin, L. Chioncel, A. I. Lichtenstein and R. A. de Groot, *Rev. Mod. Phys.* **80**, 315 (2008).
  - [4] C. Gong, L. Li, Z. Li, H. Ji, A. Stern, Y. Xia, T. Cao et al., *Nature* **546**, 265 (2017).
  - [5] B. Huang, G. Clark, E. Navarro-Moratalla, D. R. Klein, R. Cheng, K. L. Seyler, D. Zhong et al., *Nature* **546**, 270 (2017).
  - [6] Y. Deng, Y. Yu, Y. Song et al., *Nature* **563**, 94 (2018).
  - [7] F. Han, X. Yan, F. Li, H. Yu, W. Li, X. Zhong, A. Bergara and G. Yang, *Phys. Rev. B* **107**, 024414 (2023).
  - [8] D. Zhang, A. Rahman, W. Qin, X. Li, P. Cui, Z. Zhang, and Z. Zhang, *Phys. Rev. B* **101**, 205119 (2020).
  - [9] Q. Wu, Y. Zhang, Q. Zhou, J. Wang and X. C. Zeng, *J. Phys. Chem. Lett.* **9**, 4260 (2018).
  - [10] S. Gong, C. Gong, Y. Sun et al., *PNAS* **115**, 8511 (2018).
  - [11] Q. Chen, X. Zheng, P. Jiang, Y. H. Zhou, L. Zhang and Z. Zeng, *Phys. Rev. B* **106**, 245423 (2022).
  - [12] Y. J. Niu, H. F. Lv, X. J. Wu and J. L. Yang, *J. Phys. Chem. Lett.* **14**, 4042 (2023).
  - [13] S. D. Guo, Y. L. Tao, G. Wang, S. Chen, D. Huang and Y. S. Ang, *Front. Phys.* in press (2023).
  - [14] K. Lee, A. H. Dismukes, E. J. Telford et al. *Nano Lett.* **21**, 3511 (2021).
  - [15] K. Yang, G. Y. Wang, L. Liu, D. Lu and H. Wu, *Phys. Rev. B* **104**, 144416 (2021).
  - [16] Y. Guo, Y. Zhang, S. Yuan, B. Wang and J. Wang, *Nanoscale*, **10**, 18036 (2018).
  - [17] A. N. Rudenko, M. Rösner and M. I. Katsnelson, *npj Comput. Mater.* **9**, 83 (2023).
  - [18] B. I. Weintrub, Y. L. Hsieh, S. Kovalchuk, J. N. Kirchof, K. Greben, and K. I. Bolotin, *Nat. Commun.* **13**, 6601 (2022).
  - [19] P. Hohenberg and W. Kohn, *Phys. Rev.* **136**, B864 (1964); W. Kohn and L. J. Sham, *Phys. Rev.* **140**, A1133 (1965).
  - [20] G. Kresse, *J. Non-Cryst. Solids* **193**, 222 (1995).
  - [21] G. Kresse and J. Furthmüller, *Comput. Mater. Sci.* **6**, 15 (1996).
  - [22] G. Kresse and D. Joubert, *Phys. Rev. B* **59**, 1758 (1999).

- [23] J. P. Perdew, K. Burke and M. Ernzerhof, Phys. Rev. Lett. **77**, 3865 (1996).
- [24] X. Wu, D. Vanderbilt and D. R. Hamann, Phys. Rev. B **72**, 035105 (2005).
- [25] A. Togo, F. Oba and I. Tanaka, Phys. Rev. B **78**, 134106 (2008).
- [26] J. Li and R. Wu, Nano Lett. **23**, 2173 (2023).
- [27] S. D. Guo, Y. L. Tao, H. T. Guo, Z. Y. Zhao, B. Wang, G. Z. Wang and X. T. Wang, Phys. Rev. B **107**, 054414 (2023).
- [28] S. D. Guo, J. X. Zhu, G. Z. Wang et al., Phys. Rev. Materials **7**, 044604 (2023).
- [29] A. O. Fumega and J. L. Lado, Nanoscale **15**, 2181 (2023).
- [30] L. Dong, J. Lou and V. B. Shenoy, ACS Nano, **11**, 8242 (2017).
- [31] J. Tan, Y. H. Wang, Z. T. Wang, X. J. He, Y. L. Liu, B. Wang, M. I. Katsnelson and S. J. Yuan, Nano Energy **65**, 104058 (2019).
- [32] A. A. M. Noor, H. J. Kim and Y. H. Shin, Phys. Chem. Chem. Phys. **16**, 6575 (2014).
- [33] M. T. Ong and E. J. Reed, ACS Nano **6**, 1387 (2012).
- [34] Y. Guo, S. Zhou, Y. Z. Bai, and J. J. Zhao, Appl. Phys. Lett. **110**, 163102 (2017).
- [35] Y. Li, J. Deng, Y. Zhang et al., npj Comput. Mater. **9**, 50 (2023).